Progress in Natural Science: Materials International 2012;22(4):341–346

Chinese Materials Research Society

Progress in Natural Science: Materials International

www.elsevier.com/locate/pnsmi
www.sciencedirect.com

ORIGINAL RESEARCH

Fabrication of multilayer films from regenerated cellulose and graphene oxide through layer-by-layer assembly

Li Tang[b], Xiang Li[b], De Du[b], Chunju He[a,b,*]

[a]*State Key Laboratory for Modification of Chemical Fibers and Polymer Materials, Shanghai 201620, China*
[b]*College of Materials Science and Engineering, Donghua University, Shanghai 201620, China*

Received 5 April 2012; accepted 10 June 2012
Available online 16 August 2012

KEYWORDS

Regenerated cellulose;
Graphene oxide;
Layer-by-layer assembly;
Multilayer films

Abstract A key challenge in the preparation of nanoplatelet-filled polymer composites is the ability to realize the nanometer-level dispersion and the planar orientation of nanosheets in polymer matrices. In this report, multilayer films were successfully fabricated by layer-by-layer assembly of regenerated cellulose and graphene oxide, in which graphene oxide nanosheets were used as the building blocks. The thickness of 50 layer film is about 20 μm and it exhibits a high degree of smoothness. This may be attributed to the well-defined layered structure with high degree of planar orientation and nanolevel assemblies of graphene oxide nanosheets in the polymer matrices. Typical field emission scanning electron microscope images demonstrate an ordered arrangement of layers. The electrical conductivity of the multilayer films shows a remarkable increase with increasing layer of the films. A significant enhancement of mechanical properties has been achieved, that is, a 110.8% improvement of elastic modulus and a 262.5% increase of hardness respectively.

1. Introduction

Graphene-based materials have attracted tremendous attention due to the excellent properties of graphene sheets [1–7]. According to theoretical and experimental results, individual graphene nanosheets exhibit extremely high values of Young's modulus (~1 TPa), fracture strength (~130 GPa) [2], elastic modulus (~0.25 TPa) [3], thermal conductivity (~5000 W/(m K)) [4], electrical conductivity(~6000 S/cm) [5], specific surface area (theoretical limit: ~2630 m^2/g) [6], charge carrier mobility (~2×10^5 cm^2/V s) [7], etc. These properties make graphene a promising material in many applications such as

*Corresponding author at: State Key Laboratory for Modification of Chemical Fibers and Polymer Materials, Shanghai 201620, China. Tel.: +86 21 6779 2842; fax: +86 21 6779 2855.
E-mail address: chunjuhe@dhu.edu.cn (C. He).

Peer review under responsibility of Institute of Materia Medica, Chinese Academy of Medical Sciences and Chinese Pharmaceutical Association.

ELSEVIER Production and hosting by Elsevier

1002-0071 © 2012 Chinese Materials Research Society. Production and hosting by Elsevier Ltd. All rights reserved.
http://dx.doi.org/10.1016/j.pnsc.2012.06.005

photovoltaic devices, sensors [8], electrodes [9], shielding materials [10], supercapacitors [11,12], and composites [13,14].

Cellulose, the most abundant natural polymer in nature, is renewable, biodegradable, and biocompatible. Therefore, increasing attention has been paid to cellulose as an inexhaustible source of raw materials to replace petrochemically derived compounds in many applications [15]. However, cellulose is difficult to process in solution due to the strong intra- and inter-molecular hydrogen bonds. Recently, ionic liquids (IL), which are considered to be desirable green solvents, have been reported to be effective cellulose solvents. For example, 1-butyl-3-methylimidazolium chloride ([Bmim]Cl), is found to be a powerful, nonderivatizing single-component solvent which rapidly dissolves cellulose[16].

Layer-by-layer (LbL) has been widely applied to fabricate organic–inorganic nanocomposites because it is a simple, powerful, and environmental approach for assembling functional building blocks into thin films with controlled type, size, morphology, internal organization, and molecular structure. LbL assembly has been successfully driven by several different kinds of forces, such as electrostatic forces [17,18], hydrogen bonding [19–22], covalent bonding [23,24] and other weak intermolecular interactions [25,26]. Recently increasing interest has been focused on the construction of nanoscale LbL assembled materials driven by hydrogen bond formation, opening a new opportunity for the LbL technique. Although various intermolecular interactions have been used to incorporate variety of functional building blocks, it is still challenging to assemble cellulose through the LbL approach [17] due to its dissolving difficulty. In this report, we fabricated thin regenerated cellulose (RC)/graphene oxide (GO) composite films by LbL self-assembly, in which exfoliated GO nanosheets were used as building blocks. The existence of oxygen functional groups located on edges and basal plane of GO and the hydroxyl groups in RC chains makes it possible to fabricate layer-by-layer thin films by hydrogen-bonding interaction. Unlike some reports [27,28] in which the thin film was prepared by the complex vaccum-assistant self-assembly method, in this paper randomly orientated graphene/RC nanocomposite was prepared by simply solution blending, alternative deposition of RC and GO nanolayers, resulting in a uniform growth of films containing high planar orientation and good dispersion of GO. To the best of our knowledge, there are few reports about the multilayer thin films of graphene-like materials and polymer through the LbL technique.

2. Experimental

2.1. Materials

Graphite was supplied by Shanghai Yifan Graphite Co., Ltd. (Shanghai, China), with an average particle size of 150 μm and a purity of $>9\%$. Cellulose (cotton linter pulp) was obtained from Fujian Nanzhi Co., Ltd. (Fujian, China), and its viscosity-average degree of polymerization (DP) was 500. Cellulose samples were dried at 75 °C for 4 h in a vacuum oven before use. The other chemicals were analytical grade and used as obtained from Sinopharm Chemical Reagent Co., Ltd.

2.2. Preparation of graphene oxide (GO)

GO was prepared by a modified Hummers' method through acid oxidation of a natural graphite powder [29]. In a typical procedure, natural graphite (2 g) was slowly added into H_2SO_4 (46 mL) under vigorous stirring in an ice-water bath until a black slurry formed. $NaNO_3$ (1 g) and $KMnO_4$ (6 g) was gradually added with stirring while the temperature was kept below 20 °C. Subsequently, the solution was transferred to a water bath at 35 ± 2 °C and stirred for 30 min to form a thick green paste. Then, 80 mL of distilled water was slowly added (Note: caution must be exercised since this is a highly exothermic process), and the temperature was controlled below 100 °C. After 15 min, the mixture was further diluted with 300 mL distilled water and treated with 30% H_2O_2 solution (5 mL) until the cessation of gas evolution; the dark brown solution turned yellow. Finally, the mixture was filtered and washed several times with 5% HCl aqueous solution and distilled water respectively until the pH of the solution became neutral. The sample of GO was obtained as a gray powder after drying.

2.3. Fabrication of films

Briefly, [Bmim]Cl was synthesized as described in the literature [30]. A cellulose sample was dispersed in [Bmim]Cl and heated under mechanical stirring at 85 °C until a 1 wt% transparent solution was obtained for LbL assembly. Yellow–brown dispersion of GO was prepared by dissolving 20 mg of graphite oxide in 200 mL of deionized water by sonication for 30 min. Prior to deposition of the RC–GO films, the glass slides were sonicated in CCl_4 for 15 min and then rinsed with 2-propanol and deionized water. Their surface was then hydroxylated by 30 min sonication in piranha solution (mixture of 98% H_2SO_4 and 30% H_2O_2, 7:3 v/v) (caution: piranha solution reacts violently with organic compounds) and was rinsed sequentially with deionized water, methanol, 1:1 methanol/toluene and dried in an oven. The overall process of LbL deposition of thin film of $(RC/GO)_n$ as the following steps: (1) immersing the treated glass slide into 1 wt% RC for 5 min; (2) rinsing with deionized water thoroughly for 3 min and dried with air flow; (3) dipping into 0.1 mg/mL GO dispersion for 5 min; (4) rinsing with deionized water for 3 min and again dried with air flow. This procedure gave a single deposition cycle, and the cycle could then be repeated as necessary to obtain the desired number of layers $(RC/GO)_n$. In order to strengthen the junction between GO and RC matrices, film with every 10 layers were immersed into 5 vol% glutaraldehyde solution for 30 min to allow for cross-linking. A parallel pure RC film was prepared by the method as mentioned above.

2.4. Characterization

The fracture surface morphology of the composite was observed on a JSM-5600LV (JEOL, Japan) field emission scanning electron microscope (FESEM) at an accelerating voltage of 3.0 kV. The sample was fractured in liquid nitrogen and sputtered with gold for observation.

Raman spectra were recorded using a LabRam-1 B Raman spectroscope (HORIBA Jobin Yvon, France), with He–Ne laser excitation at 632.8 nm, scanning for 50 s.

Typical tapping-mode atomic force microscopy (AFM) measurements were taken using a Multimode SPM from Digital Instruments (Veeco, USA). Samples of AFM images were prepared by depositing a dispersed graphene oxide solution

($0.1\ mg\ mL^{-1}$) onto a freshly cleaved mica surface and air-drying.

The surface topography image was observed on Wyko NT9100 optical profiler (Veeco, USA).

The conductivity of the composite films was measured using a Keithley 2635 system sourcemeter (Keithley, USA).

The measurement of the mechanical properties was performed using the TriboIndenter in-situ nanomechanical test system from Hysitron, Inc. (Hysitron, USA).

3. Results and discussion

3.1. Exfoliation of graphene oxide

Graphene oxide was prepared from natural graphite powder by oxidation with $KMnO_4$ in concentrated H_2SO_4 according to modified Hummers' method. GO can be well dispersed in water at the level individual sheets in our work with many oxygen-containing functional groups. The AFM image of GO nanosheets in Fig. 1 shows GO nanosheets has the thickness of ~1.2 nm. This fact reveals the characteristics of fully exfoliated GO nanosheets.

Raman spectroscopy is strongly sensitive to the electronic structure and has been proved to be an essential tool to characterize graphite and graphene materials. The spectrum of the natural graphite shows the peak at ~1578 cm^{-1}(G band) and a very weak band at ~1345 cm^{-1} (D band), as shown in Fig. 2(a). The G band corresponds to an E_{2g} mode of graphite, which is related to the vibration of sp^2 bonded carbon atoms, while the D band is a breathing mode of k-point phonons of A_{1g} symmetry, which is associated with the vibrations of carbon atoms with dangling bonds in plane terminations of disordered graphite [31,32]. As shown in Fig. 2(b), the G band of GO broadens and shifts to 1588 cm^{-1}. Besides, the D band at 1364 cm^{-1} becomes prominent. The intensity ratio (I_D/I_G) expresses the sp^2/sp^3 carbon ratio, a measure of the extent of disorder [33], which increase from 0.13 for natural graphite to 0.88 for GO, indicating the reduction in size of the in-plane sp^2 domains. This may due to the extensive oxidation of graphite.

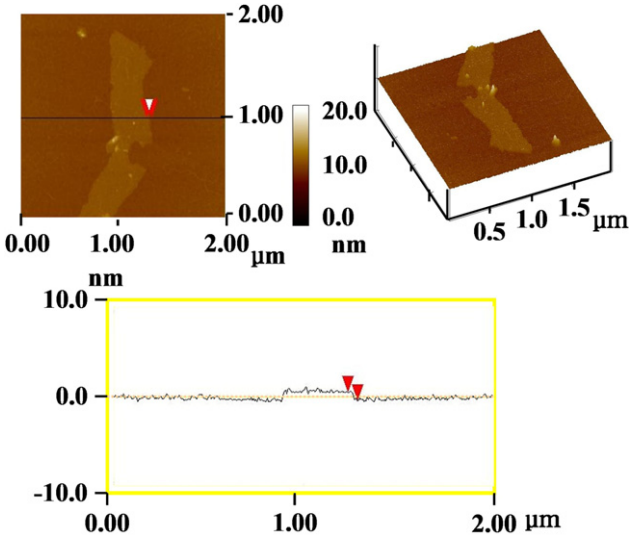

Fig. 1 A typical AFM tapping-mode image of graphene oxide nanosheets deposited onto a mica substrate from an aqueous dispersion with superimposed cross-section measurements taken along the black line, indicating a sheet thickness of ~1.2 nm.

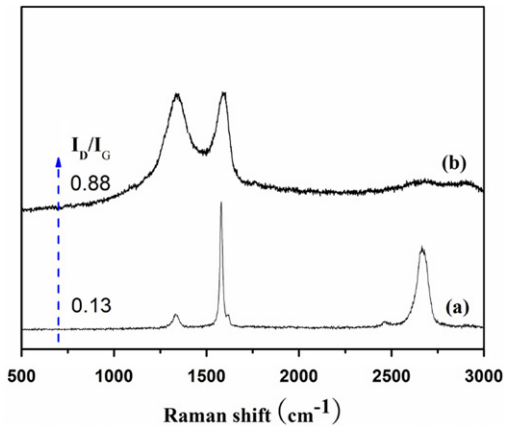

Fig. 2 Laser Raman spectra of (a) graphite, and (b) graphene oxide.

3.2. Morphology and structure of multilayer $(RC/GO)_n$ films

A traditional layer-by-layer film was prepared by immersing a glass substrate in dilute solutions of the components. RC possesses primary and secondary hydroxyl groups in its glucosamine unit, and is used in the traditional electrostatic LbL technique. Nevertheless, hydroxyl group of the quartz substrate and the oxidation functional groups of GO have been proved to form hydrogen bonds with the hydroxyl group of cellulose respectively, just as indicated schematically in Fig. 3. It is supposed that the hydrogen-bonding interactions between GO nanosheets and RC can drive the reproducible layer-by-layer composite deposition to fabricate ordered inorganic/organic periodic nanostructure. However, we have not proved the existence of hydrogen bonds using instruments, the following works will be done regarding this.

FESEM images of the $(RC/GO)_{50}$ film in Fig. 4 reveal ordered layer structure and the thickness of 50-layer film is about ~20 µm.

Optical images of $(RC/GO)_n$ thin films deposited on cleaned glass substrates are shown in Fig. 5(a), the composite films have a high level of flatness and homogeneity, and the transparency decreases with increasing deposited cycle. The highly accurate 3D surface topography for the $(RC/GO)_{50}$ are shown in Fig. 5 (b) and (c), the composite films exhibits the roughness (R_a) of ~0.21 µm and the thickness of ~20 µm, indicating a high degree of smoothness and an average thickness of ~400 nm for per layer.

3.3. Conductivity measurement

The conductivity of the $(RC/GO)_n$ thin films is shown in Fig. 6. After the oxidation of graphite, the sp^2 structure of graphite oxide was partly restored, and the conductivity of the multilayers film is enhanced with increasing number of the layers. When the layers of multilayers film increased from 10 to 50, the conductivity of the film increased by 3 times of magnitude to 1.3×10^{-4} S/m. Addition uniformly GO can cause the conductivity of the RC, probably due to the formation of conductive networks throughout the insulating RC. The enhancement of the conductivity is mainly due to its

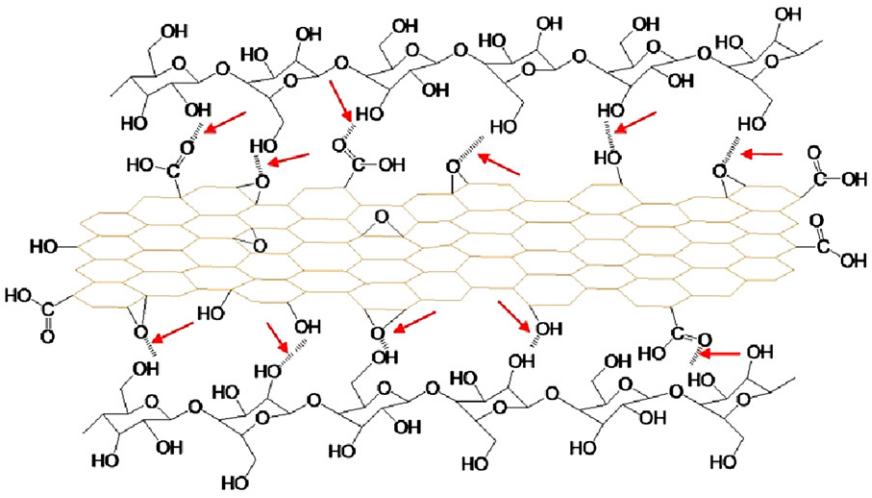

Fig. 3 Simply schematic representation of the interaction of GO surface and RC macromolecular chains, the red rows demonstrate hydrogen bonds.

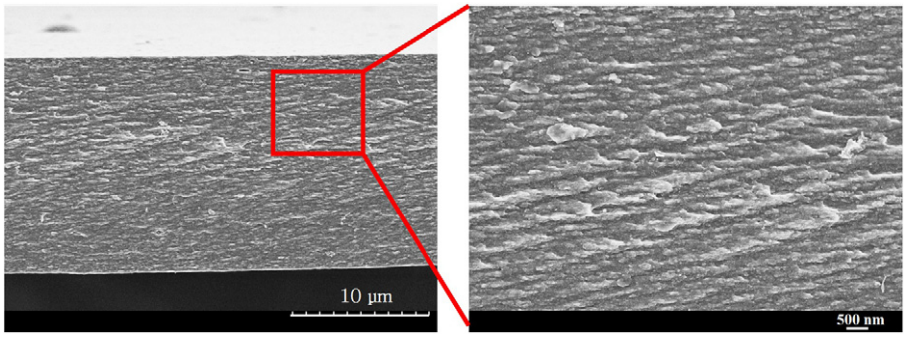

Fig. 4 FESEM images of cross section of $(RC/GO)_{50}$ composites with different magnification. 50 demonstrates layer.

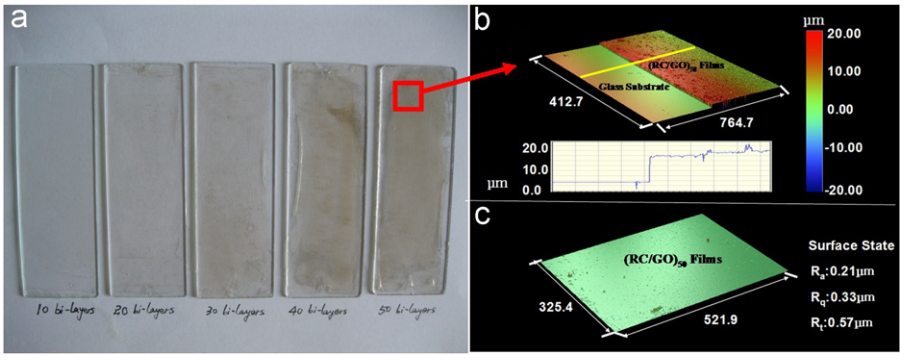

Fig. 5 (a) Optical images of $(RC/GO)_n$ composites deposited on cleaned glass substrates with gradually increasing deposited cycles, $n=10$, 20, 30, 40, and 50, and the surface topography of $(RC/GO)_{50}$ ultrathin film with the thickness (b) and the roughness (c).

higher GO content with higher layers. The conductive property of the multilayers film makes it a promising candidate for biosensor and tissue engineering applications.

3.4. *Mechanical properties of multilayer $(RC/GO)_n$ films*

Typical loading-hold-unloading curses of pure RC films and LbL assembling $(RC/GO)_n$ composite film are shown in Fig. 7. When loading, the force is incremented at constant velocities and the maximum value is 150 μm. The penetration depth represents the contributions from the elastic to plastic displacements. It is noted that the penetration depth of $(RC/GO)_{100}$ film is decreased markedly, indicating an enhancement of composite's resistance to indentation. That is, the softer material surface requires lower normal load to induce a comparable indenter penetration. When holding time with 5 s, and the peak loads are kept constant, a creep is clearly observed in the maximum hold segments for pure RC film. During unloading, the force is removed and the elastic displacement is also recovered. It is shown that the ending displacement of pure RC film is much larger than that of

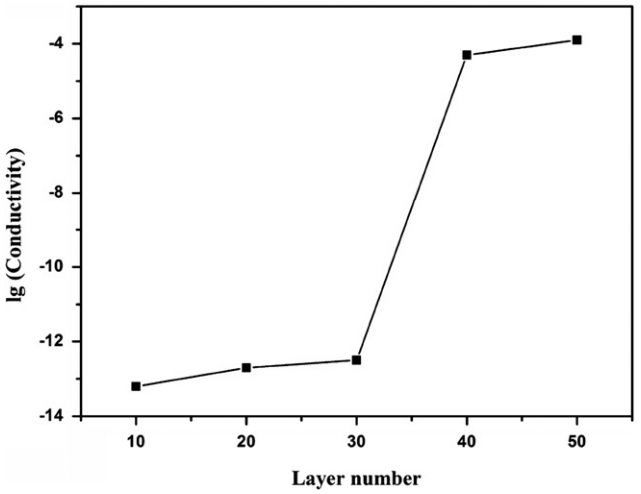

Fig. 6 Conductivity of the $(RC/GO)_n$ composites films with different layer number.

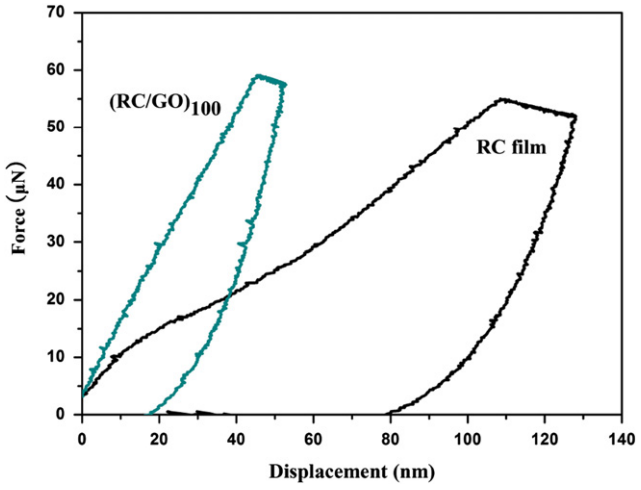

Fig. 7 Typical loading-hold-unloading curves of pure RC film and LbL assembling (RC/GO)100 film.

Table 1 Average values of elastic modulus and hardness for regenerated cellulose and nanocomposites.

Samples	E_r (GPa)	H (GPa)
pure RC films	5.55±0.03	0.24±0.02
$(RC/GO)_{100}$	11.70±0.02	0.87±0.03

$(RC/GO)_{100}$ film. Furthermore, the initial unloading stiffness of the $(RC/GO)_{100}$ film, as represented by the slope of the unloading curve, is larger than that of pure RC film, suggesting the increase of elastic modulus. The average values of elastic modulus (E_r) and hardness (H), calculated using the Oliver–Pharr method [34], are listed in Table 1. A significant enhancement of mechanical properties of LbL assembling RC/GO composites; that is, a 110.8% increase of E_r and a 262.5% improvement of H. A similar tendency for E_r and H related to graphene-based composites were also reported by Das et al., [35] an increase of 35% and 45% in the E_r and H of PVA with the addition of 0.6 wt% graphene respectively. The reasons for our remarkable increase in the mechanical properties are attributed to the nanometer-level dispersion and the strong interfacial bonding between the GO and RC matrix. The degree of structural organization by the LbL process of the nanoplatelets in the composite increases RC/GO interaction and constrains the polymer chain motion, which results in efficient load transfer between the matrix and the reinforcement phase in the composite.

4. Conclusions

In summary, the uniform thin multilayer $(RC/GO)_n$ films with high homogeneity and orientation were successfully fabricated by the layer-by-layer assembly technique driven by hydrogen-bonding interaction. The thickness of per layer is about 400 nm. The well-dispersed graphene oxide nanosheets have a high degree of planar orientation in the lamella structure films, and strong interaction between RC and GO, resulting in a significant enhancement of the mechanical properties for the LbL composites: as compared with pure RC sample the mechanical properties of multilayer $(RC/GO)_n$ films have been significantly enhanced, that is, a 110.8% improvement of elastic modulus (E_r) and a 262.5% increase of hardness (H) respectively. The electrically conductive RC/GO multilayers film with desirable degree of nanoscale orientation is one of promising candidates for advanced biochemical and electrochemical devices.

Acknowledgments

Financial support of this work is provided by the Fund of National Natural Science 51103019 and 21174027.

References

[1] A.K. Geim, K.S. Novoselov, The rise of graphene, Nature Materials 6 (2) (2007) 183–191.
[2] C. Lee, X.D. Wei, J. Hone, Measurement of the elastic properties and intrinsic strength of monolayer graphene, Science 321 (385) (2008) 385–388.
[3] C. Gomez-Navarro, M. Burghard, K. Kern, Elastic properties of chemically derived single graphene sheets, Nano Letters 8 (7) (2008) 2045–2049.
[4] A.A. Balandin, S. Ghosh, C.N. Lau, et al., Superior thermal conductivity of single-layer graphene, Nano Letters 8 (3) (2008) 902–907.
[5] X. Du, I. Skachko, E.Y. Andrei, Approaching ballistic transport in suspended graphene, Nature Nanotechnology 3 (3) (2008) 491–495.
[6] M.D. Stoller, J.H. An, R.S. Ruoff, et al., Graphene-based ultracapacitors, Nano Letters 8 (10) (2008) 3498–3502.
[7] K.I. Bolotin, K.J. Sikes, H.L. Stormer, et al., Ultrahigh electron mobility in suspended graphene, Solid State Communications 146 (9–10) (2008) 351–355.
[8] S. Ansari, E.P. Giannelis, Functionalized graphene sheet-poly (vinylidene fluoride) conductive nanocomposites, Journal of Polymer Science Part B: Polymer Physics 47 (9) (2009) 888–897.
[9] J. Yan, T. Wei, F. Wei, et al., Preparation of graphene nanosheet/carbon nanotube/polyaniline composite as electrode material for supercapacitors, Journal of Power Sources 195 (9) (2010) 3041–3045.

[10] J.J. Liang, Y. Wang, Y.S. Chen, et al., Electromagnetic interference shielding of graphene/epoxy composites, Carbon 47 (3) (2009) 922–925.
[11] Y.W. Zhu, M.D. Stoller, R.S. Ruoff, et al., Exfoliation of graphene oxide in propylene carbonate and thermal reduction of the resulting graphene oxide platelets, ACS Nano 4 (2) (2010) 1227–1233.
[12] A.V. Murugan, T. Muraliganth, A. Manthiram, Rapid facile microwave-solvothermal synthesis of graphene nanosheets and their polyaniline nanocomposites for energy storage, Chemistry of Materials 21 (21) (2009) 5004–5006.
[13] J.J. Liang, T.Y. Guo, Y.S. Chen, et al., Infrared-triggered actuators from graphene-based nanocomposites, Journal of Physical Chemistry C 113 (22) (2009) 9921–9927.
[14] X.C. Xiao, T. Xie, Y. Cheng, Self-healable graphene polymer composite, Journal of Materials Chemistry 20 (17) (2010) 3508–3514.
[15] D. Klemm, B. Heublein, H.P. Fink, Cellulose: fascinating biopolymer and sustainable raw material, Angewandte Chemie International Edition 44 (22) (2005) 3358–3393.
[16] O.A. Seoud, A. Koschella, L.C. Fidale, Application of ionic in carbohydrate chemistry: a window of opportunities, Biomacromolecules 8 (9) (2007) 2629–2647.
[17] C. Cortez, J.F. Quinn, X.J. Hao, et al., Multilayer buildup and biofouling characteristics of PSS-b-PEG containing films, Langmuir 26 (12) (2010) 9720–9727.
[18] B.S. Shim, W. Chen, N.A. Kotov, et al., Smart electronic yarns and wearable fabrics for human biomonitoring made by carbon nanotube coating with polyelectrolytes, Nano Letters 8 (12) (2008) 4151–4157.
[19] G.H. Zeng, Y.B. Xing, X. Zhang, et al., Unconventional layer-by-layer assembly of graphene multilayer films for enzyme-based glucose and maltose biosensing, Langmuir 26 (18) (2010) 15022–15026.
[20] L.Y. Wang, S.X. Cui, X. Zhang, et al., Multilayer assemblies of copolymer PSOH and PVP on the basis of hydrogen bonding, Langmuir 16 (2) (2000) 10490–10494.
[21] Y. Fu, S.L. Bai, X. Zhang, et al., Hydrogen-bonding-directed layer-by-layer multilayer assembly: reconformation yielding microporous films, Macromolecules 35 (3) (2002) 9451–9458.
[22] S.L. Bai, Z.Q. Wang, X. Zhang, Hydrogen-bonding-directed layer-by-layer films: effect of electrostatic interaction on the microporous morphology variation, Langmuir 20 (12) (2004) 11828–11832.
[23] I. Cerkez, H.B. Kocer, S.D. Worley, et al., Biocidal coatings via a layer-by-layer assembly technique, Langmuir 27 (2) (2011) 4091–4097.
[24] Y.X. Pan, B. Tong, J.B. Shi, et al., Fabrication, characterization, and optoelectronic properties of layer-by-layer films based on terpyridine-modified MWCNTs and Ruthenium(III) Ions, Journal of Physical Chemistry C 114 (7) (2010) 8040–8047.
[25] X.C. Zhang, Y.F. Wang, J. Xu, et al., Arithmetic computation using self-assembly of DNA tiles: subtraction and division, Progress in Natural Science 19 (3) (2009) 377–388.
[26] X.B. Zhao, F. Pan, J.R. Lu, Recent development of peptide self-assembly, Progress in Natural Science 18 (6) (2008) 653–660.
[27] Y.Y. Feng, Q. Xue, T. Yong, et al., A mechanically strong, flexible and conductive film based on bacterial cellulose/graphene nanocomposite, Carbohydrate Polymers 87 (1) (2012) 644–649.
[28] C.J. Kim, W. Khan, D.H. Kim, et al., Graphene oxide/cellulose composite using NMMO monohydrate, Carbohydrate Polymers 86 (2) (2011) 903–909.
[29] W.S. Hummers, R.E. Offeman, Preparation of graphitic oxide, Journal of the American Chemical Society 80 (6) (1958) 1339–1439.
[30] B. Wang, Y.F. Tang, Z.W. Wen, H.P. Wang, Dissolution and regeneration of polybenzimidazoles using ionic liquids, European Polymer Journal 45 (10) (2009) 2962–2965.
[31] F. Tuinstra, J.L. Koenig, Raman spectrum of graphite, Journal of Chemical Physics 53 (4) (1970) 1126–1130.
[32] T.C. Chieu, M.S. Dresselhaus, Raman studies of benzene-derived graphite fibers, Physical Review B 26 (2) (1982) 5867–5877.
[33] L. Alvareza, A. Righia, J.L. Sauvajola, Excitation energy dependence of the Raman spectrum of single-walled carbon nanotubes, Chemical Physics Letters 320 (5–6) (2000) 441–447.
[34] W.C. Oliver, G.M. Pharr, An improved technique for determining hardness and elastic modulus using load and displacement sensing indentation experiments, Journal of Materials Research 7 (6) (1992) 1564–1583.
[35] B. Das, K.E. Prasad, U. Ramamurty, et al., Nano-indentation studies on polymer matrix composites reinforced by few-layer graphene, Nanotechnology 20 (3) (2009) 125705–125709.